

## Crystal structure analyses of four tourmaline specimens from the Cleopatra's Mines (Egypt) and Jabal Zalm (Saudi Arabia), and the role of Al in the tourmaline group

FERDINANDO BOSI,<sup>1,\*</sup> TONČI BALIĆ-ŽUNIĆ,<sup>2</sup> AND ADEL A. SUROUR<sup>3,4</sup>

<sup>1</sup>Dipartimento di Scienze della Terra, Sapienza Università di Roma, P.le A. Moro, 5, I-00185 Rome, Italy

<sup>2</sup>Department of Geography and Geology, University of Copenhagen, Østervoldgade 10, DK-1350 Copenhagen K, Denmark

<sup>3</sup>Geology Department, Faculty of Science, Cairo University, 12613 Giza, Egypt

<sup>4</sup>Department of Mineral Resources and Rocks Faculty of Earth Sciences, King Abdulaziz University, P.O. Box 80206, 21589 Jeddah, Kingdom of Saudi Arabia

### ABSTRACT

Fe-rich “oxydravite” and dravite from the Late Proterozoic ophiolitic mélange of the Arabo-Nubian Shield, located in Egypt and Saudi Arabia, were structurally and chemically characterized by using crystal structure refinement based on single-crystal X-ray diffraction data, electron microprobe analysis, and Mössbauer spectroscopy. Structural formulae obtained by optimization procedures indicate disordering of Al, Mg, and Fe<sup>2+</sup> over the Y and Z sites, and an ordering of Fe<sup>3+</sup> at Y. The disordering can be explained by the substitution mechanisms  $2^Y\text{Mg}+^Z\text{Al}+^W\text{OH} = 2^Y\text{Al}+^Z\text{Mg}+^W\text{O}^{2-}$  and  $2^Y\text{Fe}^{2+}+^Z\text{Fe}^{3+}+^W\text{OH} = 2^Y\text{Fe}^{3+}+^Z\text{Fe}^{2+}+^W\text{O}^{2-}$ , which are consistent with reducing the mismatch in dimensions between YO<sub>6</sub> and ZO<sub>6</sub> octahedra.

To explain the Mg-Al disordering process, as well as the occurrence of B at the T site in tourmaline, analogies have been drawn between the crystal structure of tourmaline and that of lizardite. A critical constraint in both structures is the geometrical fit of the six-membered tetrahedral ring with the attached group of three YO<sub>6</sub> octahedra. In tourmaline, the disordering of Mg and Al over Y and Z relieves the strain due to the misfit in dimensions of the larger triads of edge-sharing MgO<sub>6</sub> octahedra and the smaller Si<sub>6</sub>O<sub>18</sub> tetrahedral rings. In Al-rich tourmaline, where the octahedral cluster is smaller, the strain can be relieved by incorporating B in the tetrahedra. An opposite effect is observed by substitution of Al for Si at the tetrahedral site in Mg-rich tourmaline. Because the Al radius is intermediate between those of Mg and Si, Al plays an important structural role in accommodating the potential misfit between YO<sub>6</sub>, ZO<sub>6</sub>, and TO<sub>4</sub> polyhedra. The amount of Al and its distribution in the structure strongly affects the values of the unit-cell parameters of tourmaline and yields volume variations according to a quadratic model. This results from the effect of <sup>Z</sup>Al combined with the occurrence of B at T in Al-rich tourmaline. <sup>Z</sup>Al has a greater effect than <sup>Y</sup>Al as long as Al does not fully occupy the Z site.

**Keywords:** Chemical analysis, tourmaline, crystal structure, Mössbauer spectroscopy, order-disorder, XRD data

### INTRODUCTION

Tourmaline-group minerals are complex borocyclosilicates with the general formula: XY<sub>3</sub>Z<sub>6</sub>(T<sub>6</sub>O<sub>18</sub>)(BO<sub>3</sub>)<sub>3</sub>V<sub>3</sub>W, where <sup>[9]</sup>X = Na, Ca, □ (=vacancy), K; <sup>[6]</sup>Y = Al, Fe<sup>3+</sup>, Cr<sup>3+</sup>, V<sup>3+</sup>, Mg, Fe<sup>2+</sup>, Mn<sup>2+</sup>, Cu<sup>2+</sup>, Zn, Li, Ti<sup>4+</sup>, □; <sup>[6]</sup>Z = Al, Fe<sup>3+</sup>, Cr<sup>3+</sup>, V<sup>3+</sup>, Mg, Fe<sup>2+</sup>; <sup>[4]</sup>T = Si, Al, B, Be; <sup>[3]</sup>B = B; <sup>[3]</sup>W(O1) = OH, F, O; <sup>[3]</sup>V(O3) = OH, O.

The crystal structure and crystal chemistry of this mineral group have been widely studied (e.g., Foit 1989; Hawthorne 1996; Hawthorne and Henry 1999; Bosi et al. 2005a, 2005b; Bosi and Lucchesi 2007; Lussier et al. 2008). The distribution of cations over the Y and Z non-equivalent octahedral sites is often associated with order-disorder processes. Several studies have reported a significant disorder of Al, Cr, Mg, Fe<sup>3+</sup>, and Fe<sup>2+</sup>, coupled with Mg and/or Fe<sup>2+</sup> occurring at the Z site (e.g., Hawthorne et al. 1993; Bosi et al. 2004; Bosi 2008). Although Al shows a site preference for Z, the disordering of Mg and Fe

over Y and Z also occurs for amounts of Al exceeding 6 atoms per formula unit (apfu). The Al content is one of the most important parameters in the crystal chemistry of tourmaline. Apart from H, B, and Si, Al is both the most abundant and frequent cation that occurs in tourmaline. In ranging from 0.00 apfu in povondraite to 9.00 apfu in olenite, Al varies far more than any other constituent in the tourmaline group. It is also the smallest octahedrally coordinated cation. Its content is one of the main factors determining the size of the Y, Z, and T coordination polyhedra (Bosi and Lucchesi 2007; MacDonald and Hawthorne 1995) and, as a consequence, the unit-cell parameters.

The present study was undertaken to explain one of the major problems in the crystal chemistry of tourmaline, the order-disorder phenomena involving Al, Mg, Fe<sup>3+</sup>, and Fe<sup>2+</sup>. Four tourmaline specimens from Egypt and Saudi Arabia were investigated using several different analytical approaches. To clarify the role played by Al in the tourmaline structure, spatial atomic arrangements, and the structural response to the variation of Al contents are explored.

\* E-mail: [ferdinando.bosi@uniroma1.it](mailto:ferdinando.bosi@uniroma1.it)

## GEOLOGICAL SETTING OF SAMPLES AND PARAGENESIS

Tourmaline crystals are common in areas dominated by a Pan-African ophiolitic mélange in both the Eastern Desert of Egypt and Saudi Arabia that were a single block before the opening of the Red Sea. The mélange unit comprises variable-sized mafic and ultramafic fragments set in a metasedimentary matrix made up mostly of pelitic schists. In the four investigated occurrences, tourmaline crystals are found in pegmatites and aplites, and in surrounding pelitic schists and enclosed ultramafic fragments. The tourmaline crystals investigated in this work were collected at three localities in Egypt and one in Saudi Arabia.

In the Egyptian occurrences, tourmaline is found in pegmatites and metasediments associated with gem-quality beryl (emerald) at the famous, ancient Cleopatra's Mines in the Eastern Desert (Grundmann and Morteani 1993, 2008; Harrell 2004). Mineral parageneses in the Egyptian occurrences can be summarized as follows: quartz-feldspars-garnet-biotite-phlogopite-tourmaline±beryl (in the case of pegmatites and pelitic schists) or tremolite-actinolite-tourmaline-apatite (in the case of metapyroxenite). Three different tourmaline crystals were sampled from the latter paragenesis, from Wadi Sikait, Wadi Umm Sleimat, and Wadi Umm Ad Deba'a (samples SKT, ST, and DT, respectively) where tourmaline crystals up to 15 cm long can be found. The age of tourmaline and the coexisting emerald is 580–520 Ma based on K-Ar age of the accompanying phlogopite (Surour et al. 2002).

The collected tourmaline crystals from the Saudi Arabian occurrence at Jabal Zalm attain a maximum length of only 5 cm, and the assemblage containing beryl and phlogopite is not present. The single investigated tourmaline crystal from there (sample SA) originates from chloritized metapyroxenite pockets in much larger masses of serpentinites derived from a dunite-peridotite protolith of the Jabal Zalm area of Saudi Arabia. The post-orogenic felsic intrusions consisting of pegmatites and aplites were enriched in B and were responsible for the development of tourmaline in both the ultramafic rocks (particularly the more permeable retrograded serpentinites and chloritized rocks) and the enclosing metasediments. Most likely, the Zalm tourmaline is genetically related to these aplite dikes, which are the sole felsic intrusions cutting the metapyroxenites. Tourmaline was introduced into the metapyroxenite during a late event post-dating serpentinization and chloritization during the Pan-African orogeny, and is typically associated with clinocllore, magnetite, and apatite. Well-formed octahedral magnetite crystals are common inclusions in tourmaline; these resulted from the release of Fe from actinolite that could not be accommodated in clinocllore.

## ANALYTICAL AND CRYSTAL STRUCTURAL PROCEDURES

### Single-crystal structural refinement

Four representative crystal fragments of tourmaline were selected for X-ray diffraction measurements on a Bruker-AXS four-circle diffractometer equipped with a Smart 1000CCD area detector (6.25 × 6.25 cm active detection area, 512 × 512 pixels) and a flat graphite monochromator, using MoK $\alpha$  radiation from a fine-focus sealed X-ray tube. The sample-to-detector distance was 4 cm. A total of 2800 exposures per sample (step = 0.2°, time/step = 10 s) covering a full reciprocal sphere were collected. SMART software was used for data collection. The orientation of the crystal lattice was determined from 700 to 1000 strong reflections ( $I > 50 \sigma$ )

evenly distributed in reciprocal space, and used for subsequent integration of all recorded intensities. Data integration and reduction (for polarization and Lorentz effects) were performed with the SAINT+ program. An absorption correction was accomplished with a semi-empirical method assuming an ellipsoidal shape of the fragments (North et al. 1968). Final unit-cell parameters were refined from 4000 recorded reflections with  $I > 10 \sigma$ , in the range  $8^\circ < 2\theta < 71^\circ$ . No violations of  $R3m$  symmetry were noted.

Structural refinement was carried out with the SHELXL-97 program (Sheldrick 1997). Starting coordinates were taken from Bosi (2008). Variable parameters were scale factor, extinction coefficient, atomic coordinates, site scattering values expressed as mean atomic number (for X, Y, and Z sites) and atomic displacement factors. The X and Z sites were modeled using Na and Al scattering factors, respectively. The occupancies of the Y site were obtained considering the presence of Mg vs. Fe. For samples DT, SKT, and ST, the occupancy of Al at the Z site was fixed to 1 because refinement with unconstrained Z occupancy showed no significant deviations from this value. In contrast, the Z-site occupancy was freely refined for sample SA. The T and B sites were modeled, respectively, with Si and B scattering factors and with fixed occupancy of 1 because refinement with unconstrained occupancies showed no significant deviations from this value. Three full-matrix refinement cycles with isotropic displacement parameters for all atoms were followed by anisotropic cycles until convergence was attained. No correlations over 0.7 between the parameters were observed at the end of refinement. All crystals were refined as merohedral/racemic twins. We first made non-twinned refinements, but for crystal ST, the SHELXL program automatically estimated a Flack-x parameter of about 0.4. This value provides strong evidence of inversion twinning, and thus it was essential to refine the Flack-x parameter as a full-matrix parameter according to a twin law  $\mathbf{R} = (-1 \ 0 \ 0, 0 \ -1 \ 0, 0 \ 0 \ -1)$ . The statistical index  $wR2$  of crystal ST decreased accordingly (from 6.12 to 5.99). The amount of the structure racemically twinned varies from 4% in crystal SKT to 37% in crystal ST, as suggested by the refined Flack parameters (Table 1), that is, the presence of twinning in the samples SA, DT, and SKT is doubtful because of the low values of the refined Flack parameter they show. Nonetheless, all samples were refined on the same basis to preserve the full comparability of the data, including the Flack parameter.

Table 1 lists crystal data, data collection information, and refinement details, and Table 2 gives the fractional atomic coordinates, equivalent isotropic displacement parameters, mean bond lengths, and mean atomic numbers at the cation sites in the structure. Tables 3<sup>1</sup> and 4<sup>1</sup> contain relevant bond lengths and anisotropic displacement parameters, respectively.

### Electron microprobe analysis

Electron microprobe analyses were obtained by wavelength dispersive spectroscopy, using a JEOL JXA-8200 Superprobe at the University of Copenhagen, operating at an accelerating potential of 15 kV and a sample current of 15 nA, with a beam diameter of 5  $\mu\text{m}$ . For raw data reduction, the PAP computer program was applied (Pouchou and Pichoir 1984). Natural and synthetic standards were used: corundum (Al), rutile (Ti), wollastonite (Si and Ca), hematite (Fe), olivine (Mg), albite (Na), orthoclase (K), apatite (F), and synthetic MnTiO<sub>3</sub>, ZnO, Cr<sub>2</sub>O<sub>3</sub>, and V<sub>2</sub>O<sub>5</sub> (Mn, Zn, Cr, and V, respectively). Each element determination was accepted after checking that the intensity of the analyzed standard before and after each determination did not change by more than 1%. The chemical compositions are the averages of 10 spot analyses, performed along two orthogonal traverses, and their low standard deviations indicate compositional homogeneity (Table 5). In accordance with the documented very low concentration of Li in dravitic samples (Dyar et al. 1998) and the absence of the other Li-containing minerals in the samples, the Li content was assumed to be insignificant. K, Zn, Mn, and Cr were in concentrations below their detection limits.

The magnetite inclusion in sample SA has the following formula (apfu):  ${}^{\text{IV}}(\text{Fe}^{3+})_{\text{VI}}(\text{Fe}_{1.00}^{2+}\text{Fe}_{0.95}^{3+}\text{V}_{0.03}\text{Al}_{0.02})\text{O}_4$ , with Mn, Zn, Cr, and Ti < 0.01 apfu.

### Mössbauer spectroscopy (MS)

With the purpose of determining Fe<sup>3+</sup>/ΣFe ratios and the Fe partitioning in the tourmaline specimens, four <sup>57</sup>Fe Mössbauer spectra were obtained on absorbers prepared by placing finely ground crystals between plastic foil in a ca. 2.5 mm

<sup>1</sup> Deposit item AM-10-023, Tables 3 and 4 (bond lengths and anisotropic displacement parameters). Deposit items are available two ways: For a paper copy contact the Business Office of the Mineralogical Society of America (see inside front cover of recent issue) for price information. For an electronic copy visit the MSA web site at <http://www.minsocam.org>, go to the *American Mineralogist* Contents, find the table of contents for the specific volume/issue wanted, and then click on the deposit link there.

**TABLE 1.** X-ray diffraction data of the four analyzed tourmaline specimens

	SA	DT	SKT	ST
<b>Crystal data</b>				
Space group	<i>R3m</i>	<i>R3m</i>	<i>R3m</i>	<i>R3m</i>
Z	3	3	3	3
a (Å)	15.9730(6)	15.9533(8)	15.9534(8)	15.959(8)
c (Å)	7.1952(3)	7.2007(4)	7.2121(4)	7.205(5)
V (Å <sup>3</sup> )	1589.8(1)	1587.1(1)	1589.6(1)	1589.2(2)
Crystal size (mm)	0.45 × 0.35 × 0.2	0.2 × 0.15 × 0.1	0.6 × 0.4 × 0.3	0.3 × 0.3 × 0.2
<b>Data collection and refinement</b>				
Radiation, MoKα (Å)	0.71073	0.71073	0.71073	0.71073
Temperature (K)	298(2)	298(2)	298(2)	298(2)
Total number of frames	2900	2900	2900	2900
μ (mm <sup>-1</sup> )	2.093	1.677	1.675	1.675
F(000)	1667	1639	1639	1639
Range for data collection, θ (°)	4.08–35.72	4.09–35.99	4.08–35.76	4.08–35.72
Reciprocal space range hkl	(-21 ≤ h ≤ 25) (-25 ≤ k ≤ 25) (-11 ≤ l ≤ 11)	(-23 ≤ h ≤ 25) (-25 ≤ k ≤ 24) (-11 ≤ l ≤ 11)	(-25 ≤ h ≤ 25) (-25 ≤ k ≤ 25) (-11 ≤ l ≤ 9)	(-26 ≤ h ≤ 22) (-25 ≤ k ≤ 25) (-11 ≤ l ≤ 11)
Set of measured reflections	7370	7446	7472	7302
Unique reflections	1682	1713	1589	1690
R <sub>int</sub> (%)	4.22	3.87	3.43	3.94
Extinction coefficient	0.0001(2)	0.0001(2)	0.0005(2)	0.0011(3)
Flack parameter	0.06(2)	0.10(3)	0.04(4)	0.37(4)
wR2 (%)	4.67	5.24	5.41	5.99
R1 (%) all data	1.73	2.37	2.14	2.31
R1 (%) for I > 2σ <sub>I</sub>	1.72	2.27	2.13	2.30
Goof	1.073	1.025	1.080	1.100
Largest diff. peak and hole (e <sup>-</sup> /Å <sup>3</sup> )	0.47 and -0.50	0.66 and -0.48	0.41 and -0.27	0.42 and -0.29

**TABLE 2.** Fractional coordinates (x,y,z) and equivalent isotropic displacement factors (U<sub>eq</sub>) for atoms in the four analyzed tourmaline specimens

Site	X	Y	Z	B	T	O1(W)	O2	O3(V)	O4
<b>SA</b>									
x	0	0.12361(3)	0.29816(2)	0.10999(6)	0.19198(2)	0	0.06093(4)	0.26545(10)	0.09283(5)
y	0	x/2	0.26164(2)	2x	0.19007(2)	0	2x	x/2	2x
z	0.22368(19)	0.63449(6)	0.61106(6)	0.45395(21)	0	0.77614(32)	0.48373(17)	0.51059(16)	0.07030(16)
U <sub>eq</sub> (Å <sup>2</sup> )	0.0171(4)	0.0097(1)	0.00699(9)	0.0081(2)	0.00637(7)	0.0200(4)	0.0131(2)	0.0134(2)	0.0113(2)
m.b.l. (Å)	2.678	2.032	1.927	1.376	1.624				
m.a.n.	12.1(1)	17.89(7)	13.21(4)	5	14				
<b>DT</b>									
x	0	0.12420(4)	0.29796(3)	0.10977(7)	0.19183(2)	0	0.06078(5)	0.26364(12)	0.09306(5)
y	0	x/2	0.26151(3)	2x	0.18994(2)	0	2x	x/2	2x
z	0.22964(23)	0.63398(8)	0.61121(7)	0.45429(26)	0	0.77350(33)	0.48581(20)	0.51068(20)	0.07133(20)
U <sub>eq</sub> (Å <sup>2</sup> )	0.0164(4)	0.0086(2)	0.00637(8)	0.0071(3)	0.00565(7)	0.0141(4)	0.0120(3)	0.0139(3)	0.0109(2)
m.b.l. (Å)	2.679	2.019	1.930	1.375	1.622				
m.a.n.	11.06(9)	15.08(6)	13	5	14				
<b>SKT</b>									
x	0	0.12499(3)	0.29816(2)	0.10986(6)	0.19181(2)	0	0.06094(5)	0.26443(11)	0.09301(5)
y	0	x/2	0.26167(2)	2x	0.18992(2)	0	2x	x/2	2x
z	0.23655(25)	0.63295(8)	0.61208(7)	0.45607(25)	0	0.77334(34)	0.48663(20)	0.51163(21)	0.07072(19)
U <sub>eq</sub> (Å <sup>2</sup> )	0.0208(5)	0.0093(2)	0.00714(8)	0.0075(2)	0.00634(7)	0.0142(2)	0.0120(2)	0.0142(2)	0.0108(2)
m.b.l. (Å)	2.685	2.022	1.931	1.374	1.620				
m.a.n.	10.8(1)	14.61(6)	13	5	14				
<b>SA</b>									
x	0	0.12478(4)	0.29809(3)	0.10976(7)	0.19184(2)	0	0.06089(5)	0.26463(13)	0.09296(6)
y	0	x/2	0.26162(3)	2x	0.18995(2)	0	2x	x/2	2x
z	0.23203(25)	0.63304(9)	0.61193(8)	0.45493(27)	0	0.77394(37)	0.48582(21)	0.51144(21)	0.07116(21)
U <sub>eq</sub> (Å <sup>2</sup> )	0.0180(5)	0.0096(2)	0.00732(9)	0.0080(3)	0.00657(8)	0.0145(4)	0.0120(3)	0.0142(3)	0.0112(2)
m.b.l. (Å)	2.681	2.025	1.931	1.374	1.620				
m.a.n.	10.9(1)	14.62(7)	13	5	14				

Note: For the cation sites the mean bond length (m.b.l.) and mean atomic number (m.a.n.) are also given.

circular aperture of a Pb disk. The spectra were collected at room temperature using a conventional spectrometer system operated in constant acceleration mode with a nominal 10 mCi <sup>57</sup>Co/Rh point source. Spectral data were recorded for the velocity range -4.5 to +4.5 mm/s in a multichannel analyzer using 1024 channels. After velocity calibration against a spectrum of high-purity α-iron foil (0.25 mm thick), the raw data were reduced to 512 channels and then folded to 256 channels. The folded spectra of all samples indicated the presence of non-magnetic absorptions. Samples SA and ST also showed peaks at ca. -4 and -1 mm/s indicating the presence of an additional magnetic phase in the spectra. Consequently, a second spectrum was recorded for samples SA and ST in the range -10 to +10 mm/s to assess amount and identity of this species. Inspection of the latter spectra showed that the non-magnetic absorption (tourmaline) is associated with the magnetic

absorption. The latter corresponds, according to Mössbauer parameters, to hematite (absorption area of ca. 23 and 6% in SA and ST, respectively) and magnetite (ca. 16 and 3% in SA and ST, respectively). The same material used for MS was also used for an X-ray powder diffraction experiment, which confirmed the presence of hematite and magnetite. This result is consistent with the chemical composition of the Fe-rich phase included in sample SA (see EMPA section).

The original spectra were fitted assuming Lorentzian peak shape, using a least-squares fitting program (Jernberg and Sundqvist 1983). Reduced χ<sup>2</sup> was considered as a parameter to evaluate the best fit. Three to five doublets were used to fit the tourmaline spectra (Fig. 1) in accordance with models already used in the literature, and the resulting χ<sup>2</sup> were <1. The measured hyperfine parameters are reported in Table 6. Differential recoil-free fraction (f) contributions were not

**TABLE 5.** Chemical composition of the four analyzed tourmaline specimens

Sample	wt%				Sample	apfu			
	SA	DT	SKT	ST		SA	DT	SKT	ST
SiO <sub>2</sub>	35.09(15)	36.32(32)	37.38(25)	37.35(11)	Si	5.82(5)	5.94(7)	6.04(6)	6.07(5)
TiO <sub>2</sub>	0.45(3)	0.76(21)	0.44(8)	0.43(4)	Ti <sup>4+</sup>	0.06(1)	0.09(3)	0.05(1)	0.05(1)
B <sub>2</sub> O <sub>3</sub> *	10.47	10.62	10.75	10.69	B	3.00	3.00	3.00	3.00
Al <sub>2</sub> O <sub>3</sub>	32.11(35)	32.75(59)	32.32(25)	32.32(15)	Al	6.28(7)	6.32(10)	6.16(6)	6.19(5)
V <sub>2</sub> O <sub>5</sub>	0.09(2)	0.08(3)	0.05(1)	0.07(3)	V <sup>3+</sup>	0.01(0)	0.01(0)	0.01(0)	0.01(0)
FeO	9.72(26)	3.71(17)	3.49(12)	2.89(12)	Fe <sup>3+</sup>	0.41(2)	0.08(1)	0.03(1)	0.04(1)
MgO	5.96(7)	8.71(19)	9.43(14)	9.43(14)	Fe <sup>2+</sup>	0.94(3)	0.43(2)	0.44(2)	0.35(2)
CaO	1.04(7)	1.07(13)	0.60(10)	0.53(12)	Mg	1.47(2)	2.13(5)	2.27(4)	2.28(4)
Na <sub>2</sub> O	2.19(7)	2.15(6)	2.50(9)	2.46(12)	Ca	0.18(1)	0.19(2)	0.10(2)	0.09(2)
F	—	—	0.09(4)	0.13(5)	Na	0.71(2)	0.68(2)	0.78(3)	0.78(4)
H <sub>2</sub> O*	3.12	3.16	3.32	3.22	F	—	—	0.05(2)	0.06(2)
O=F	—	—	-0.04	-0.05	OH	3.46(16)	3.45(17)	3.58(16)	3.49(15)
Total	100.24	99.34	100.33	99.46	OH+F	3.46	3.45	3.62	3.55
FeO†	6.75	3.11	3.25	2.57	e <sup>-</sup> <sub>chemical</sub>	244.0	232.6	231.2	229.9
Fe <sub>2</sub> O <sub>3</sub> †	3.31	0.67	0.27	0.36	e <sup>-</sup> <sub>structural</sub>	244.0	233.3	231.7	231.7

Notes: Number of ions calculated on basis of 31 (O, OH, F). Digits in parentheses are estimated errors (1 $\sigma$ ). Standard error for oxides and F (wt%) are derived from repeated analyses on individual crystal, whereas standard errors for B<sub>2</sub>O<sub>3</sub> and H<sub>2</sub>O were assumed at 5%. Standard error for ions was calculated by error propagation theory. e<sup>-</sup><sub>chemical</sub> and e<sup>-</sup><sub>structural</sub> = number of electrons per formula unit derived from chemical and structural analysis.

\* Calculated by stoichiometry.

† From MS data (Table 6).

**TABLE 2.—EXTENDED**

O5	O6	O7	O8	H3
<b>SA</b>				
0.18441(10)	0.19632(6)	0.28533(6)	0.20924(6)	0.254(6)
x/2	0.18626(6)	0.28525(6)	0.26999(6)	x/2
0.09202(16)	0.77652(11)	0.07917(11)	0.44026(12)	0.399(13)
0.0117(2)	0.0092(1)	0.0089(1)	0.0099(1)	0.17(4)
<b>DT</b>				
0.18420(11)	0.19540(6)	0.28521(7)	0.20911(7)	0.217(8)
x/2	0.18541(7)	0.28503(6)	0.26982(7)	x/2
0.09227(19)	0.77734(14)	0.07908(13)	0.44031(14)	0.391(14)
0.0107(2)	0.0085(2)	0.0081(2)	0.0095(2)	0.23(5)
<b>SKT</b>				
0.18422(10)	0.19569(6)	0.28485(6)	0.20915(6)	0.237(6)
x/2	0.18566(6)	0.28482(6)	0.27002(6)	x/2
0.09152(19)	0.77781(14)	0.07950(13)	0.44148(14)	0.385(12)
0.0109(2)	0.0094(1)	0.0090(1)	0.0102(2)	0.15(3)
<b>SA</b>				
0.18418(11)	0.19568(7)	0.28498(7)	0.20913(7)	0.245(5)
x/2	0.18568(7)	0.28495(7)	0.26992(7)	x/2
0.09195(20)	0.77830(15)	0.07957(13)	0.44128(15)	0.385(10)
0.0112(2)	0.0095(2)	0.0088(2)	0.0102(2)	0.09(2)

considered because there are no published data for  $f$  values in tourmaline. Errors were estimated at  $\pm 0.02$  mm/s for isomer shift ( $\delta$ ), quadrupole splitting ( $\Delta E_Q$ ), and peak width ( $\Gamma$ ), and  $\pm 1$ –3% for absorption areas due to doublet overlap. The principal oxidation state observed is Fe<sup>2+</sup>, followed by Fe<sup>3+</sup>. Fe<sup>2+</sup> with delocalized electron (ED) was only observed in sample SA.

## RESULTS

### Determination of atomic proportions

Contents of FeO and Fe<sub>2</sub>O<sub>3</sub> were obtained from Fe<sup>2+</sup>/Fe<sup>3+</sup> ratios measured by MS. In agreement with structure refinement

results, the boron content was assumed to be stoichiometric in all samples (B = 3.00 apfu). In fact, both the mean atomic number and the mean bond lengths of B and T are consistent with both the B site fully occupied by boron and no or negligible amount of B at the T site. The OH content can then be calculated by charge balance with the assumption T+Y+Z = 15.00 apfu. The atomic proportions were calculated on this assumption (Table 5). The good match between the number of electrons per formula unit derived from chemical and structure analysis (Table 5) supports this procedure.

According to the classification of Hawthorne and Henry (1999), these tourmaline specimens belong to the alkali group, since the X site is dominated by Na (from 0.79 to 0.68 apfu). The Al content is nearly constant in all samples (average value of 6.23 apfu), whereas Mg and Fe vary. In particular, the amount of Mg (2.30–1.47 apfu) is larger than the amount of Fe (1.35–0.40 apfu), with Fe<sup>2+</sup> (0.94–0.35 apfu) exceeding Fe<sup>3+</sup>. The last is present in relatively high concentrations in sample SA (Fe<sup>3+</sup> = 0.41 apfu), whereas Fe<sup>3+</sup> < 0.10 apfu in the other samples. On the basis of the concentrations of OH and O<sup>2-</sup> at the W site, these tourmalines may be classified as Fe-rich “oxydravite” (samples SA and DT) and Fe-rich dravite (samples SKT and ST).

### Determination of site populations

To convert crystal-chemical and structure refinement results into accurate site populations, experimental and calculated data from atomic distributions should be optimized. By using a quadratic program to minimize the residuals between calculated and observed data (relative to chemical and structure analyses) and the ionic radii reported in Bosi and Lucchesi (2007), the cation distribution of the T, Y, and Z sites was obtained for the present specimens. All residuals between calculated and observed data (such as mean atomic number, mean bond lengths, atomic proportions) are within the analytical error. More details about

**TABLE 6.** Mössbauer parameters of the four analyzed tourmaline specimens

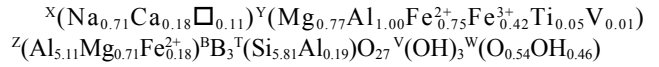
Iron valence	Sample	SA		DT		SKT		ST		Assignment
		Value	Fe*	Value	Fe*	Value	Fe*	Value	Fe*	
Fe <sup>2+</sup>	$\delta$	1.10		1.08		1.09		1.09		
	$\Delta E_Q$	2.49		2.46		2.46		2.45		
	$\Gamma$	0.13		0.13		0.14		0.15		
	% area	35±1	0.47	58±1	0.29	73±1	0.35	65±1	0.26	Y1 site
Fe <sup>2+</sup>	$\delta$	1.10		1.07		1.06		1.07		
	$\Delta E_Q$	2.16		2.02		1.95		1.94		
	$\Gamma$	0.17		0.27		0.27		0.27		
	% area	13±3	0.18	26±1	0.13	20±1	0.09	24±1	0.10	Y2 site
Fe <sup>2+</sup>	$\delta$	1.20								
	$\Delta E_Q$	1.15								
	$\Gamma$	0.33								
	% area	13±2	0.18							Z site
Fe <sup>3+</sup>	$\delta$	0.47		0.40		0.62		0.43		
	$\Delta E_Q$	0.59		0.58		0.68		0.52		
	$\Gamma$	0.27		0.36		0.40		0.44		
	% area	23±1	0.30	16±2	0.08	7±2	0.03	11±2	0.04	Y site
Fe ED	$\delta$	0.67								
	$\Delta E_Q$	1.46								
	$\Gamma$	0.20								
	% area	16±3	0.22							Y-Y sites

Notes:  $\delta$  (isomer shift),  $\Delta E_Q$  (quadrupole splitting), and  $\Gamma$  (peak width) are in mm/s. Errors on these parameters are  $\pm 0.02$  mm/s. ED = electron delocalization (namely Fe<sup>2.5+</sup>).

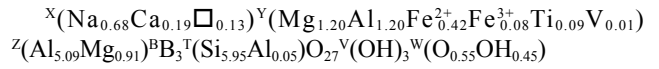
\* Proportion of Fe (apfu) in tourmaline site derived from the absorption area (% area) of the tourmaline phase

the optimization procedure may be found in Bosi and Lucchesi (2004). The optimized structural formulae are as follows:

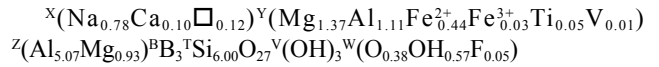
(1) sample SA



(2) sample DT



(3) sample SKT



(4) sample ST

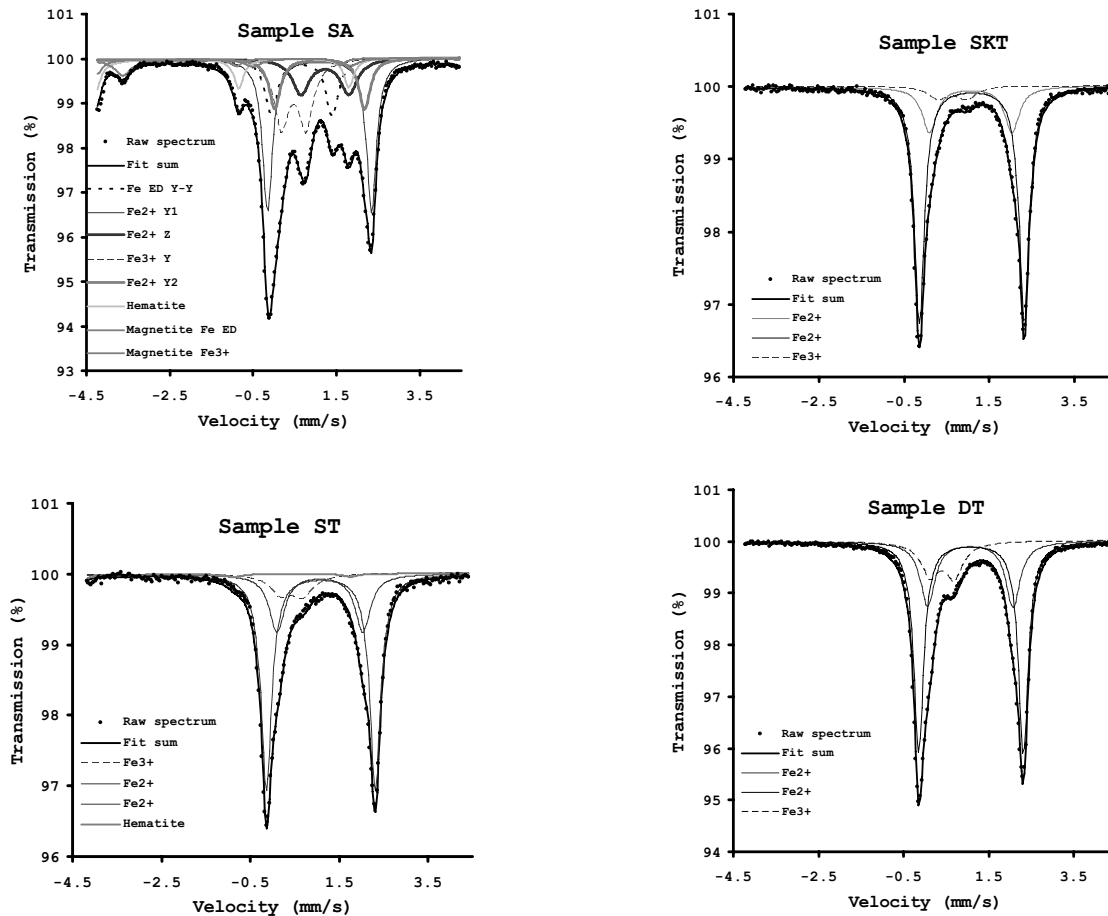
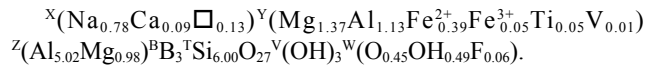


**FIGURE 1.** Room-temperature Mössbauer spectra of samples SA, ST, DT, and SKT. In samples SA and ST, the data were recorded in the velocity range  $-10$  to  $10$  mm/s to evaluate the hematite-magnetite contribution to the tourmaline spectrum (only a selected region from  $-4.5$  to  $4$  mm/s is displayed). In sample ST, the magnetic contribution was below the analytical uncertainty (ca. 3%). ED = electron delocalization.

These formulae, which are consistent with those obtained by using the optimizing method of Wright et al. (2000), show disordering of Al over the Y, Z, and T sites as well as disordering of Mg over Y and Z, and a strong ordering of Fe<sup>2+</sup> and Fe<sup>3+</sup> at the Y site. The only exception to this cation-distribution trend is observed in sample SA: although Fe<sup>2+</sup> seems to prefer the Y site, a significant amount of Fe<sup>2+</sup> is also accommodated at Z.

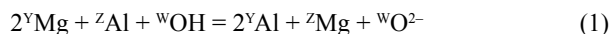
### Mössbauer data

The tourmaline specimens here studied all possess Fe in octahedral coordination. For all samples, doublets assigned to Fe<sup>2+</sup> show nearly constant  $\delta$  values (from 1.1 to 1.2 mm/s) and are distinguished by their  $\Delta E_Q$  values representing Fe<sup>2+</sup> with different nearest-neighbor coordination environments: ~2.5 mm/s (Y site, named Y1), ~2 mm/s (Y site, named Y2), and ~1.2 mm/s (Z site). The last is only observed in sample SA. The Fe<sup>3+</sup> doublets present in all samples are characterized by  $\delta$  ranging from 0.4 to 0.6 mm/s and  $\Delta E_Q$  ranging from 0.5 to 0.7 mm/s. Although their assignment to Y or Z sites is problematic due to close overlap of the absorption doublets, Fe<sup>3+</sup> was assigned to Y on the basis of structural formulae. Electron delocalization doublets, namely Fe<sup>2.5+</sup>—observed at  $\delta = 0.67$  mm/s and  $\Delta E_Q = 1.46$  mm/s in sample SA—were assigned to the interaction between Fe<sup>2+</sup>-Fe<sup>3+</sup> located in Y-Y on the basis of the structural formula. Furthermore, it should be noted that the Mössbauer data used to characterize the relative site occupancies for Fe, when combined with chemical data, yielded absolute occupancies in agreement with those derived from optimized structural formulae. Table 6 summarizes the Fe site assignment models. These models are consistent with the Fe site assignments and the Mössbauer parameters reported in Andreozzi et al. (2008) and Bosi (2008).

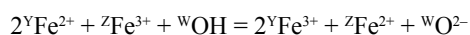
## DISCUSSION

### Order-disorder mechanisms and structural misfit between Y and Z

Ideal ordered tourmaline (such as the end-member dravite) is expected to have the divalent cations (e.g., Mg) and trivalent cations (e.g., Al) ordered at the Y and Z sites, respectively. In contrast, the structural formulae above show a disordering of Al and Mg over the Y and Z sites. Furthermore, sample SA also shows Fe<sup>2+</sup> disordered over Y and Z. In accordance with bond valence theory, Hawthorne (1996) showed that the occurrence of Mg at Z and Al at Y is due to disorder associated with the occurrence of O<sup>2-</sup> at the W site, expressed by the substitution mechanism



and also predicted that arguments similar to those used to explain the Mg-Al disordering apply to their Fe<sup>2+</sup>-Fe<sup>3+</sup> analogues. On this basis, the substitution mechanism



may be proposed, and both of them are tentatively applied to the present samples. Results are convincing, since local arrangements around the W site, such as  ${}^Y(2R^{3+}+R^{2+})$  where  $R^{3+}$

= (Al, Fe<sup>3+</sup>) and  $R^{2+}$  = (Mg, Fe<sup>2+</sup>), match  ${}^W\text{O}^{2-}$  contents within analytical error. The standard error related to the difference in the  ${}^YR^{3+}/2$  and  ${}^W\text{O}^{2-}$  ( $\Delta$ ) can be calculated as the square root of the sum of squares of errors of  ${}^YR^{3+}/2$  and  ${}^W\text{O}^{2-}$  ( $=\sigma_{\text{OH}}$ ):  $\sigma_{\Delta} = [(\sigma_{R^{3+}/2})^2 + (\sigma_{\text{O}^{2-}})^2]^{1/2}$ . Assuming that  $\Delta$  is distributed around zero according to a normal distribution, the uncertainty in  $\Delta$  at the 95% confidence level is given by  $\pm 2$  standard errors. In line with this statistical criterion,  $\Delta$  values ( $<0.2$  apfu) are within the analytical error ( $2\sigma_{\Delta} > 0.2$  apfu). As a consequence, the Mg-Al disordering mechanism applies to all samples and, in addition, the Fe<sup>2+</sup>-Fe<sup>3+</sup> relation explains both the presence of Fe<sup>2+</sup> at the Z site and the Fe<sup>3+</sup> fully ordered at the Y site in sample SA.

From a steric point of view, these disordering mechanisms involve the incorporation of smaller trivalent cations into Y (Al, Fe<sup>3+</sup>) and larger divalent cations into Z (Mg, Fe<sup>2+</sup>). As a result, the mean bond length  $\langle\text{Y-O}\rangle$  decreases and  $\langle\text{Z-O}\rangle$  increases. Such mechanisms are, therefore, consistent with findings of Bosi and Lucchesi (2007) and Bosi (2008) on the structural stability of tourmaline. Disordering of  $R^{2+}$  and  $R^{3+}$  over Y and Z is necessary for the tourmaline structure to reduce the structural misfit between YO<sub>6</sub> and ZO<sub>6</sub> by maintaining the difference between  $\langle\text{Y-O}\rangle$  and  $\langle\text{Z-O}\rangle$  smaller than ca. 0.15 Å (Bosi and Lucchesi (2007). Because  $\langle\text{Y-O}\rangle$  is always greater than  $\langle\text{Z-O}\rangle$  in tourmaline, and because of the small size of the Al<sup>3+</sup> cation, the disordering of Al (Mg and Fe<sup>2+</sup>) over Y and Z decreases free energy and increases the stability of the structure; that is, ordered atomic configurations appear to be less stable than disordered ones, which leads to Al occupying non-equivalent crystallographic sites.

### Tetrahedral ring vs. octahedral triads

The tourmaline structure is characterized by groups of XO<sub>9</sub>, YO<sub>6</sub>, TO<sub>4</sub>, and BO<sub>3</sub> polyhedra connected to each other through ZO<sub>6</sub> octahedra. The type of linkage between the ditrigonal ring of six tetrahedra (T<sub>6</sub>O<sub>18</sub>) and the three-equivalent YO<sub>6</sub> octahedra (Fig. 2) is similar to that observed in the lizardite structure.

As in the lizardite case, in which the edges of Mg-octahedra are somewhat larger than the distances between apical O atoms in the tetrahedral ring, a metric misfit between the three YO<sub>6</sub> octahedra and an ideal hexagonal T<sub>6</sub>O<sub>18</sub> ring occurs in the dravite structure (Y = Mg and T = Si). As in the layer silicates, this misfit leads to tensions in the bonds. Relief of misfit can be achieved by

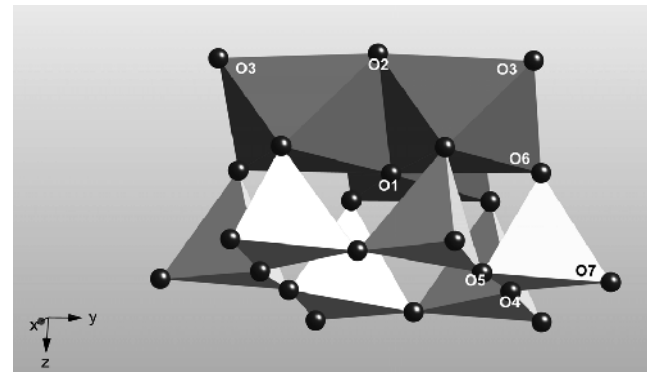


FIGURE 2. The attachment of an Y<sub>3</sub>O<sub>13</sub> octahedral triplet to a T<sub>6</sub>O<sub>18</sub> tetrahedral ring in the crystal structure of tourmaline.

substitution of Al for Si and Mg. In tourmaline, the disordering  ${}^Y\text{Mg}+{}^Z\text{Al} = {}^Y\text{Al}+{}^Z\text{Mg}$  has a similar effect by shortening Y-O bond lengths as well as shortening  $\langle\text{O-O}\rangle$  distances. As a result, the disordering of Mg and Al over Y and Z relieves the strain due to the misfit in dimensions of the larger triad of edge-sharing  $\text{MgO}_6$  octahedra and the smaller tetrahedral ring  $\text{Si}_6\text{O}_{18}$ . It seems reasonable to suppose that an ordered dravite is less stable than a disordered dravite in which Y is occupied by  $2\text{Mg}+\text{Al}$  and Z by  $5\text{Al}+\text{Mg}$ . This cation disordering occurs in combination with  ${}^W\text{O}^{2-}$  (Hawthorne 1996) and can be connected to the substitution mechanism (1). The disorder shifts the equation to the right side and in this way the greater abundance of “oxydravite” with respect to dravite (e.g., Novák et al. 2004) may be explained.

A similar mechanism for relief of misfit between  $\text{YO}_6$  and  $\text{T}_6\text{O}_{18}$  also applies to the Al-rich tourmaline containing a large excess of boron (i.e.,  $\text{Al} > 7$  and  $\text{B} > 3$  apfu). Usually, such Al-rich tourmaline has the Z site fully occupied by Al, the Y site dominated or fully occupied by Al, and the T site characterized by both B and Si. It has been shown that the  ${}^T\text{B}$  content increases with increasing Al at the Y site because of the bond valence requirements (e.g., Schreyer et al. 2002). Also, in this case, the size match of  $\text{YO}_6$  and  $\text{T}_6\text{O}_{18}$  is a reasonable explanation. The incorporation of Al at Y causes a reduction in size of the three equivalent  $\text{YO}_6$  octahedra in conjunction with the reduction in size of the B-substituted tetrahedral ring. Conversely, because an expansion in size of  $\text{YO}_6$  may occur via incorporation of  ${}^Y\text{Mg}$ , an opposite effect is observed by substitution of Al for Si at the T site. Such a substitution, in fact, enlarges the  $\langle\text{T-O}\rangle$  bond length as often observed in dravite and uvite (e.g., MacDonald and Hawthorne 1995).

Finally, recent studies suggest that high-pressure and low-temperature favor the incorporation of B into the T site, whereas by increasing the temperature the amount of  ${}^T\text{B}$  decreases (e.g., Marler et al. 2002; Ertl et al. 2008). This B behavior can be explained in terms of the constraints of geometrical fitting. The

T-O bond ( $\text{T} = \text{Si}^{4+}, \text{B}^{3+}$ ) is stronger than the  ${}^Y\text{Al-O}$  bond, and it can be expected that an increase in temperature results in a greater increase in the size of  ${}^Y\text{AlO}_6$  relative to  $\text{T}_6\text{O}_{18}$ . As a result, the three equivalent  ${}^Y\text{AlO}_6$  octahedra would no longer fit with the  $\text{T}_6\text{O}_{18}$  ring, thus explaining the decrease in B content at the T site with increasing temperature. Conversely, an increase in pressure would result in overall bond contraction (with different degrees of contraction of T-O and Y-O); i.e., pressure has the inverse effect on T-O and  ${}^Y\text{Al-O}$  bonds, resulting in a greater decrease in the  ${}^Y\text{AlO}_6$  size relative to  $\text{T}_6\text{O}_{18}$ . Therefore, increased  ${}^T\text{B}$  content can be promoted by increasing pressure. There is also another effect, connected to the rotation of tetrahedra. Foit (1989) and Bosi and Lucchesi (2007) reported a strong negative correlation between the tetrahedral angle rotation and  $\langle\text{Y-O}\rangle$ , showing that as  $\langle\text{Y-O}\rangle$  decreases, the closer O6 atoms approach to the threefold axis, and the larger are tetrahedral rotations about the O4-O5 edge connecting the bridging O atoms. Figure 3 shows that the tetrahedral angle rotation is positively correlated with  ${}^T\text{B}$ . As a consequence, a contraction of the  $\text{YO}_6$  octahedra can be accommodated by a rotation of the tetrahedral ring as well as by an incorporation of B at T.

#### Variation of the unit-cell parameters in the tourmaline group

Usually, variations in lattice parameters, as well as in cell volume, are determined by the size of the main constituting cations in the structure. In Al-rich tourmaline, unit-cell volume and B contents at the T site show a good correlation (e.g., Marler et al. 2002; Ertl et al. 2008).  $\text{Al}^{3+}$  is a key cation in the tourmaline structure and is accommodated mainly at Z, and to a lesser extent at Y and least at T. Consequently, it is expected that the amount of Al and its distribution within the structure strongly affect the values of the unit-cell parameters of tourmaline.

Unit-cell parameter  $c$  is negatively correlated with the amount of  ${}^Z\text{Al}$  (Fig. 4). The quadratic fit of this correlation can

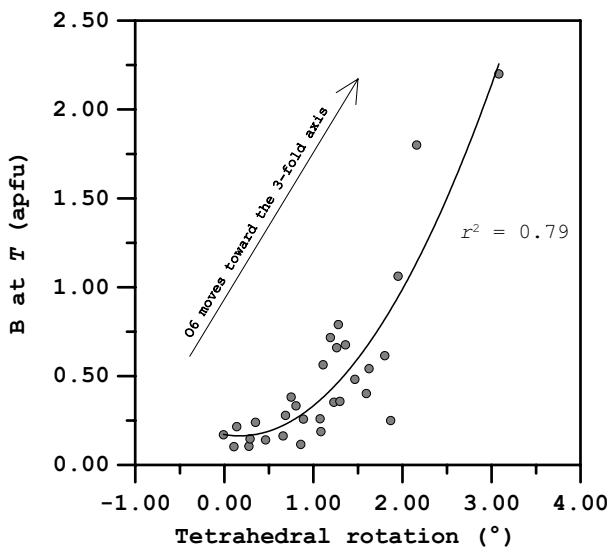


**FIGURE 3.** Tetrahedral rotation vs.  ${}^T\text{B}$ , showing a quadratic variation. The tetrahedral angle rotation is measured as the angle between (0001) and the line from O7 normal to the O4-O5 edge. Data from Bosi and Lucchesi (2007), Lussier et al. (2008), and Ertl et al. (2007).

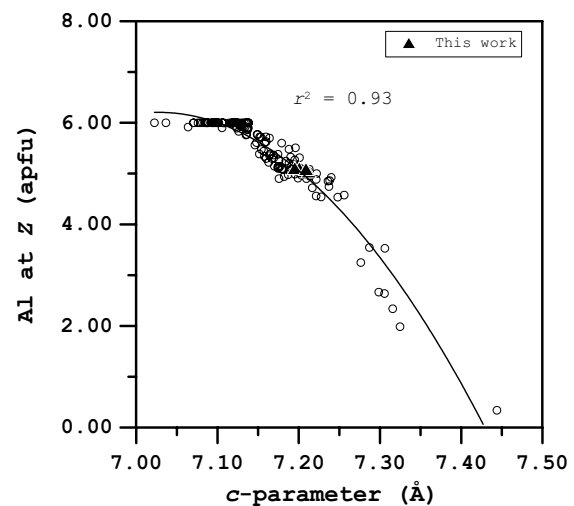


**FIGURE 4.** Variation in the  $c$  cell parameter as a function of Al at the Z site. Plots obtained using 146 data sets: 4 tourmalines from the present study, 127 from literature (see references in Bosi and Lucchesi 2007), 2 from Bosi (2008), 2 from Schreyer et al. (2002), 9 from Lussier et al. (2008), and 2 from Ertl et al. (2007, 2008).

be explained in the following way: (1) for  ${}^Z\text{Al}$  ranging from 0.00 to 4.00 apfu,  $c$  variations are mainly due to substitution  ${}^Z\text{Al} \leftrightarrow {}^Z\text{R}^{3+}$ , such as in the “oxy-chromodravite” compositional range; (2) for  ${}^Z\text{Al}$  ranging from 4.00 to 6.00 apfu,  $c$  variations are mainly due to order-disorder substitution  ${}^Z\text{Al} \leftrightarrow {}^Z\text{R}^{2+}$ , such as in “oxy-dravite” compositional range; and (3) for  ${}^Z\text{Al} = 6.00$  apfu,  $c$ -parameter variations are mainly due to variation of  ${}^Y\text{Al}$ , such as in the elbaite/olenite compositional range. In the third case, in fact, the amount of  ${}^Y\text{Al}$  is negatively correlated with unit-cell parameter  $c$  (Fig. 5). The quadratic fit of this correlation can be mainly related to the order-disorder substitution (1), which increases  $c$ . The correlation between  ${}^Y\text{Al}$  and  $c$  is in fact better defined by a linear model ( $r^2 = 0.79$ ) for tourmalines with  ${}^Z\text{Al} = 6$  apfu (Fig. 5). From Figures 4 and 5, it can be concluded that: (1) the tourmalines in which the Z site is fully occupied by Al have  $c$  parameters smaller than  $\sim 7.14$  Å, and a larger  $c$  parameter cannot be explained without assuming that cations larger than Al occur at the Z site; (2) the variation of the unit-cell parameter  $c$  depends more on  ${}^Z\text{Al}$  than on  ${}^Y\text{Al}$ . This strict dependence may be explained by the arrangement of spiral chains of Z sites around the  $3_1$  axis, i.e., parallel to the  $c$  axis. Conversely, the plane of triads of edge-sharing  $\text{YO}_6$  octahedra is parallel to the  $a$  axis. We can see that  ${}^Y\text{Al}$  and unit-cell parameter  $a$  are negatively correlated (Fig. 6). The quadratic fit of this correlation is mainly due to increase of the  ${}^T\text{B}$  content in Al-rich tourmalines, which decreases  $\langle\text{T-O}\rangle$ , i.e., the size of the  $\text{T}_6\text{O}_{18}$  ring that is arranged parallel to the  $a$  axis. Finally, Figure 7 displays the relationships of  ${}^Y\text{Al}$  and  ${}^Z\text{Al}$  with the unit-cell volume ( $V_{\text{cell}}$ ), and the relationship between  $V_{\text{cell}}$  and Al contents ( $\text{Al}_{\text{tot}}$ ). From Figure 7, it is immediately apparent that the variation between  $V_{\text{cell}}$  and  $\text{Al}_{\text{tot}}$  from 0.00 to 6.00 apfu is mainly dictated by  ${}^Z\text{Al}$  (through a variation similar to that observed with the  $c$  parameter), whereas variation between  $V_{\text{cell}}$  and  $\text{Al}_{\text{tot}}$  from 6.00 to 9.00 apfu is mainly dictated by  ${}^Y\text{Al}$  (through a variation similar to that observed with the  $a$  parameter). The quadratic form of  $V_{\text{cell}}$  vs.  $\text{Al}_{\text{tot}}$  reflects the varying contribution of three groups of polyhedra  $\text{ZO}_6$ ,  $\text{YO}_6$ , and  $\text{TO}_4$  to  $V_{\text{cell}}$ .

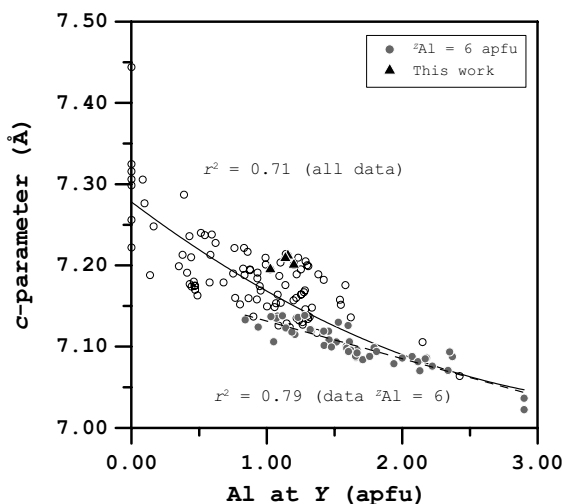


FIGURE 5. Variation in the  $c$  cell parameter as a function of Al at the Y site. The same sources of data as for Figure 4.

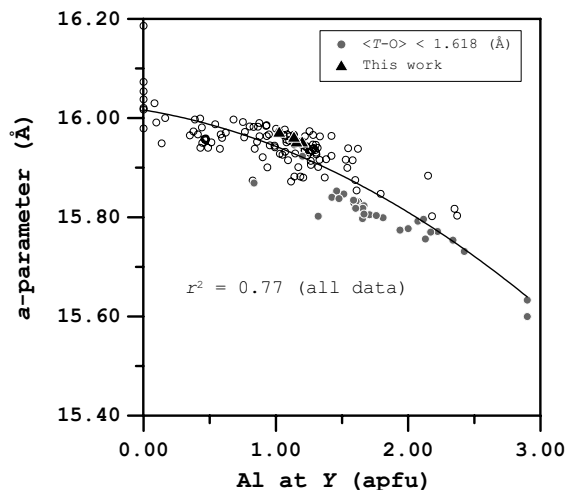


FIGURE 6. Variation in the  $a$  cell parameter as a function of Al at the Y site. As  $\langle\text{Si-O}\rangle = 1.619$  Å (Bosi and Lucchesi 2007),  $\langle\text{T-O}\rangle$  less than 1.618 Å reflects a significant presence of small cations like B. The same sources of data as for Figure 4.

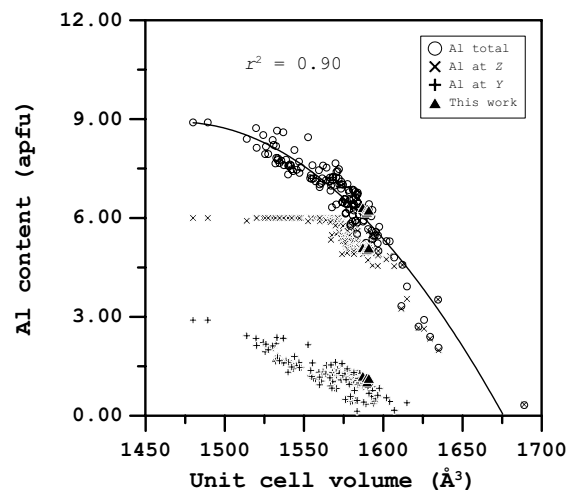


FIGURE 7. Plot of the unit-cell volume vs. the Al content showing that the quadratic correlation between  $V_{\text{cell}}$  and Al total is largely due to the correlations between  $V_{\text{cell}}$  and  ${}^Z\text{Al}$  for Al total  $< 6$  apfu and  $V_{\text{cell}}$  and  ${}^Y\text{Al}$  for Al total  $> 6$  apfu. The same sources of data as for Figure 4.

In conclusion, Al substitutions occurring at diverse crystallographic sites in the tourmaline structure yield volume variations according to a quadratic model, which results from the effect of  ${}^Z\text{Al}$  combined with the occurrence of B at T in Al-rich tourmaline.  ${}^Z\text{Al}$  has a greater effect than  ${}^Y\text{Al}$  as long as Al does not fully occupy the Z site. Due to the ionic radius of  $\text{Al}^{3+}$ , which is intermediate between those of  $\text{Mg}^{2+}$  and  $\text{Si}^{4+}$ , Al plays an important structural role in accommodating the potential misfit between  $\text{YO}_6$ ,  $\text{ZO}_6$ , and  $\text{TO}_4$  polyhedra in the crystal chemistry of the tourmaline group.

#### ACKNOWLEDGMENTS

Financial support from the Nordic Mineralogical Network is gratefully acknowledged. The authors thank Berit Wenzel (University of Copenhagen) for

careful microprobe analyses, Henrik Skogby (Swedish Museum of Natural History) for helping in the collection and interpretation of the Mössbauer spectra, and John Bailey for the careful reading and helpful comments on the content and grammar of the text. The authors thank Edward Grew, Franklin F. Foit, and an anonymous reviewer for comments that improved the quality of this manuscript.

### REFERENCES CITED

- Andreozzi, G.B., Bosi, F., and Longo, M. (2008) Linking Mössbauer and structural parameters in elbaite-schorl-dravite tourmalines. *American Mineralogist*, 93, 658–666.
- Bosi, F. (2008) Disorder of Fe<sup>2+</sup> over octahedrally coordinated sites of tourmaline. *American Mineralogist*, 93, 1647–1653.
- Bosi, F. and Lucchesi, S. (2004) Crystal chemistry of the schorl-dravite series. *European Journal of Mineralogy*, 16, 335–344.
- (2007) Crystal chemical relationships in the tourmaline group: Structural constraints on chemical variability. *American Mineralogist*, 92, 1054–1063.
- Bosi, F., Lucchesi, S., and Reznitskii, L. (2004) Crystal chemistry of the dravite-chromdravite series. *European Journal of Mineralogy*, 16, 345–352.
- Bosi, F., Agrosi, G., Lucchesi, S., Melchiorre G., and Scandale, E. (2005a) Mn-tourmaline from island of Elba (Italy). *Crystal chemistry. American Mineralogist*, 90, 1661–1668.
- Bosi, F., Andreozzi, G.B., Federico, M., Graziani, G., and Lucchesi, S. (2005b) Crystal chemistry of the elbaite-schorl series. *American Mineralogist*, 90, 1784–1792.
- Dyar, M.D., Taylor, M.E., Lutz, T.M., Francis, C.A., Guidotti, C.V., and Wise, M. (1998) Inclusive chemical characterization of tourmaline: Mössbauer study of Fe valence and site occupancy. *American Mineralogist*, 83, 848–864.
- Ertl, A., Hughes, J.M., Prowatke, S., Ludwig, T., Brandstätter, F., Körner, W., and Dyar, M.D. (2007) Tetrahedrally-coordinated boron in Li-bearing olenite from “mushroom” tourmaline from Momeik, Myanmar: structure and chemistry. *Canadian Mineralogist*, 45, 891–899.
- Ertl, A., Tillmanns, E., Ntaflos, T., Francis, C., Giester, G., Korner, W., Hughes, J.M., Lengauer, C., and Prem, M. (2008) Tetrahedrally coordinated boron in Al-rich tourmaline and its relationship to the pressure-temperature conditions of formation. *European Journal of Mineralogy*, 20, 881–888.
- Foit Jr., F.F. (1989) Crystal chemistry of alkali-deficient schorl and tourmaline structural relationships. *American Mineralogist*, 74, 422–431.
- Grundmann, G. and Morteani, G. (1993) Smaragdminen der Cleopatra: Zabara, Sikait und Umm Kabo in Ägypten. *Lapis*, 7–8, 27–39.
- (2008) Multi-stage emerald formation during Pan-African regional metamorphism: The Zabara, Sikait, Umm Kabo deposits, South Eastern desert of Egypt. *Journal of African Earth Sciences*, 50, 168–187.
- Harrell, J.A. (2004) Archeological geology of the world’s first emerald mine. *Geoscience Canada*, 31, 69–76.
- Hawthorne, F.C. (1996) Structural mechanisms for light-element variations in tourmaline. *Canadian Mineralogist*, 34, 123–132.
- Hawthorne, F.C. and Henry, D. (1999) Classification of the minerals of the tourmaline group. *European Journal of Mineralogy*, 11, 201–215.
- Hawthorne, F.C., MacDonald, D.J., and Burns, P.C. (1993) Reassignment of cation occupancies in tourmaline: Al-Mg disorder in the crystal structure of dravite. *American Mineralogist*, 78, 265–270.
- Jernberg, P. and Sundqvist, T. (1983) A versatile Mössbauer analysis program. Uppsala University, Institute of Physics (UIIP-1090).
- Lussier, A.J., Aguiar, P.M., Michaelis, V.K., Kroeker, S., Herwig, S., Abdu, Y., and Hawthorne, F.C. (2008) Mushroom elbaite from the Kat Chay mine, Momeik, near Mogok, Myanmar: I. Crystal chemistry by SREF, EMPA, MAS NMR and Mössbauer spectroscopy. *Mineralogical Magazine*, 72, 747–761.
- MacDonald, D.J. and Hawthorne, F.C. (1995) The crystal chemistry of Si ↔ Al substitution in tourmaline. *Canadian Mineralogist*, 33, 849–858.
- Marler, B., Borowski, M., Wodara, U., and Schreyer, W. (2002) Synthetic tourmaline (olenite) with excess boron replacing silicon in the tetrahedral site: II. Structure analysis. *European Journal of Mineralogy*, 14, 763–771.
- North, A.C.T., Phillips, D.C., and Mathews, F.S. (1968) A semi-empirical method of absorption correction. *Acta Crystallographica*, A24, 351–359.
- Novák, M., Povondra, P., and Selway, J.B. (2004) Schorl-oxy-schorl to dravite-oxy-dravite tourmaline from granitic pegmatites; examples from the Moldanubicum, Czech Republic. *European Journal of Mineralogy*, 16, 323–333.
- Pouchou, J.L. and Pichoir, F. (1984) A new model for quantitative X-ray microanalysis. I. Application to the analysis of homogeneous samples. *La Recherche Aérospatiale*, 3, 13–36.
- Schreyer, W., Hughes, J.M., Bernhardt, H.J., Kalt, A., Prowatke, S., and Ertl, A. (2002) Reexamination of olenite from the type locality: Detection of boron in tetrahedral coordination. *European Journal of Mineralogy*, 14, 935–942.
- Sheldrick, G.M. (1997) SHELXL-97-1. Program for crystal structure determination. University of Göttingen, Germany.
- Surour, A.A., Takla, M.A., and Omar, S.A. (2002) EPR spectra and age determination of beryl from the Eastern Desert of Egypt. *Annals of the Geological Survey of Egypt*, 25, 389–400.
- Wright, S.E., Foley, J.A., and Hughes, J.M. (2000) Optimization of site occupancies in minerals using quadratic programming. *American Mineralogist*, 85, 524–531.

MANUSCRIPT RECEIVED JULY 27, 2009

MANUSCRIPT ACCEPTED DECEMBER 2, 2009

MANUSCRIPT HANDLED BY EDWARD GREW